

Article

Leaf Vein-Inspired Bionic Design Method for Heat Exchanger Infilled with Graded Lattice Structure

Haoyu Deng ¹, Junpeng Zhao ^{1,*} and Chunjie Wang ²

¹ School of Mechanical Engineering and Automation, Beihang University, Beijing 100191, China; dhaoyu@buaa.edu.cn

² State Key Laboratory of Virtual Reality and Systems, Beihang University, Beijing 100191, China; wangcj@buaa.edu.cn

* Correspondence: zhaojunpeng@buaa.edu.cn

Abstract: Due to its excellent performance and high design freedom, the lattice structure has shown excellent capabilities and considerable potential in aerospace and other fields. This paper proposes a method to map the biometric model to the lattice structure. Taking leaf veins as bionic objects, they are used to generate a bionic design with a gradient lattice structure to improve the performance of a heat exchanger. In order to achieve the above goals, this article also proposes a leaf vein model and a mapping method that combine the leaf vein model with the lattice structure. A series of transient thermal finite element simulations was conducted to evaluate and compare the heat dissipation performance of different designs. The analysis results show that the combination of the bionic design and the lattice structure effectively improves the heat dissipation performance of the lattice structure heat exchanger. The results indicate that the application of bionic design in lattice structure design has feasibility and predictable potential.

Keywords: bionic design; lattice structure; heat transfer analysis; heat exchanger



Citation: Deng, H.; Zhao, J.; Wang, C. Leaf Vein-Inspired Bionic Design Method for Heat Exchanger Infilled with Graded Lattice Structure. *Aerospace* **2021**, *8*, 237. <https://doi.org/10.3390/aerospace8090237>

Academic Editor: Rosario Pecora

Received: 23 July 2021

Accepted: 24 August 2021

Published: 30 August 2021

Publisher's Note: MDPI stays neutral with regard to jurisdictional claims in published maps and institutional affiliations.



Copyright: © 2020 by the authors. Licensee MDPI, Basel, Switzerland. This article is an open access article distributed under the terms and conditions of the Creative Commons Attribution (CC BY) license (<https://creativecommons.org/licenses/by/4.0/>).

1. Introduction

Because of their excellent mechanical properties and multifunctionality, lattice structures have received widespread attention in both academia and industry. The lattice structure has a variety of topological configurations, and each unit can be defined by different parameters, making the lattice structure have higher designability than the conventional metal foam [1].

Since the concept of lattice structure was put forward, its ability to dissipate heat has been widely studied. Studies on the thermal performance [2], effective thermal conductivity [3,4], as well as applications [5,6] of the lattice materials have been performed based on the theory of metal foam [7–10]. Wang et al. [11] developed a lattice Boltzmann method-based computational model to predict the effective thermal conductivity of lattice structures. Ho et al. applied periodic lattice of Rhombi-Octet unit cell to the design of key cooling components. The simulation and experimental results show that the periodic lattice structure improves the thermal performance of the structure [12,13]. Shen et al. [14] replaced pin fins of wedge-shaped channels with a Kagome lattice structure, which enhanced the heat dissipation performance by 20~35%. Based on the principle of thermodynamics, Deng and Wang [15] developed an efficient method to calculate the effective thermal conductivity of the X-type lattice structure. At the same time, the distribution of the lattice structure in the heat exchanger is optimized. On the other hand, Sypeck [16] reported the application of lattice structure in various fields, including a multifunctional heat exchanger with a lattice core. Yan et al. [17] applied the X-type lattice core material to the design of the disc brake system to improve its cooling performance.

At the same time, inspired by biological structure, scholars attempted to find design directions from nature to improve the performance of heat dissipation and heat resistance.

A variety of biological characteristics have been used as bionic objects to improve the work efficiency of key component by heat transfer enhancement [18,19], micro-scale structure optimization [20–23], and reducing surface resistance [24–26]. When nutrients and water are transported from the root of the leaf to all parts, the leaf veins play a key role as shown in Figure 1. The process of nutrient transportation is similar to that of heat dissipation in a structure with concentrated heat load. Zhao et al. [27] proposed a new flat-plate heat pipe with leaf vein structure and studied the influence of the fractal angles of the vein structure. It is shown that under the optimal fractal angle, the overall efficiency of the structure can be 40% higher than that of the structure without bionic design.



Figure 1. Leaf veins in nature, photos are taken by the first author.

Although the application of bionic design has effectively improved the performance of key components, most of them are used in traditional structures, and there are few combined applications with lattice structures. This paper proposes a leaf vein-inspired bionic design method for heat exchanger infilled with graded-density lattice. The heat exchanger [16] shown in Figure 2 is used to demonstrate the effectiveness of the proposed bionic design method, where the skin of the exchanger forms an inner cavity filled by spatially-varying lattice structure cells.

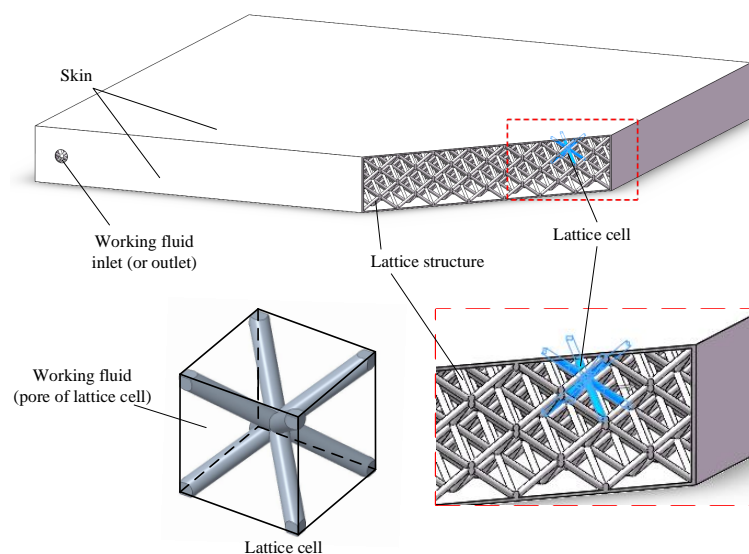


Figure 2. A typical heat exchanger with lattice structure.

For each lattice structure cell, the pores of the lattice structure are filled with working fluid, which can flow directionally in the inner cavity of the exchanger and conduct thermal convection at the surface of lattice structure. The working process of this kind of heat exchanger is shown in Figure 3.

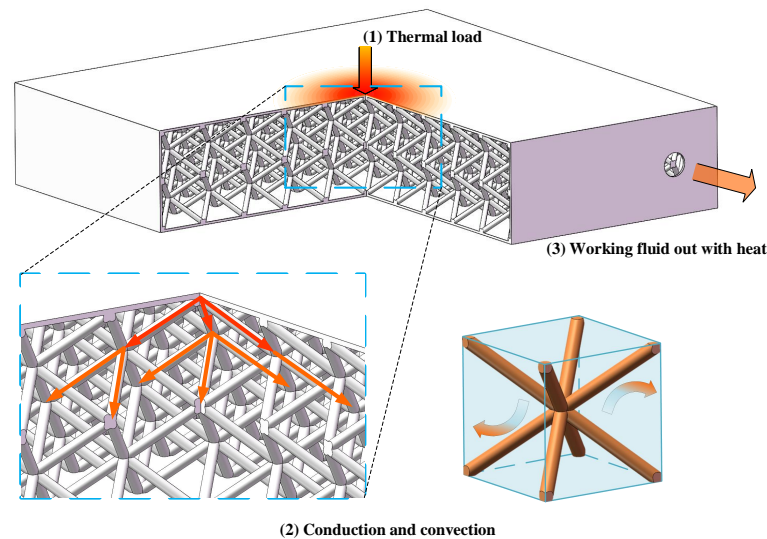


Figure 3. Working process of heat exchanger with lattice structure. (The direction of the arrow indicates the direction of heat transfer).

- (1) Local temperature variety occurs on the exchanger under thermal load.
- (2) Heat is transferred from the local part to the whole structure and working fluid by heat conduction and convection.
- (3) Heat is finally carried out of the heat exchanger by the working fluid.

In this paper, by combining bionic characteristics with lattice structure, a lattice structure with graded density, rather than uniform density, is generated to optimize the heat dissipation components and achieve improved heat dissipation efficiency.

The layout of this paper is organized as follows. Section 2 introduces the mathematical model of heat transfer in lattice cell, vein models, and mapping methods for bionic design. Section 3 introduces the numerical simulation method and models employed in this work. Section 4 presents numerical examples to demonstrate the advantages of the bionic designs. Finally, the conclusions are summarized in Section 5.

2. Models and Methods

2.1. Mathematical Model of Heat Transfer

This paper focuses on the influence of lattice structure design on heat transfer. When heat is transferred in lattice structure, each lattice cell can be equivalent to a continuous material with the same mass and conduction properties. Then, the three-dimensional heat conduction can be written as

$$\frac{\partial}{\partial x} \left(k_{e,xx} \frac{\partial T}{\partial x} \right) + \frac{\partial}{\partial y} \left(k_{e,yy} \frac{\partial T}{\partial y} \right) + \frac{\partial}{\partial z} \left(k_{e,zz} \frac{\partial T}{\partial z} \right) + \dot{q} = \rho_e c_e \frac{\partial T}{\partial \tau} \quad (1)$$

where T is temperature and $\partial T/\partial x$, $\partial T/\partial y$, and $\partial T/\partial z$ are the temperature gradient in x , y , and z directions, respectively; $\partial T/\partial \tau$ is the rate of change of temperature over time; $k_{e,xx}$, $k_{e,yy}$, and $k_{e,zz}$ represent the equivalent thermal conductivity of the equivalent material in x , y , and z directions, respectively, ρ_e and c_e are the density and specific heat capability of the equivalent continuous material, respectively; and \dot{q} is energy generated per unit volume.

According to the theory of heat conduction, the physical quantity $\alpha_e = k_e/(\rho_e c_e)$ is the equivalent thermal diffusivity of the material. When the value of α_e is large, the diffuse

of heat in the structure is fast. Thus, it is desired to design lattice structures with large value of α_e .

When the lattice structure is BCC type (also called X-type) [28] (as shown in Figure 4) and all members in the lattice cell are cylinders of same radius r_m , the equivalent heat conductivity of the unit cell can be obtained as follows [15]:

$$\begin{aligned} k_{e,xx} &= \frac{4A_m k_m}{\sqrt{(l_{\text{cell},x})^2 + (l_{\text{cell},y})^2 + (l_{\text{cell},z})^2}} \frac{l_{\text{cell},x}}{l_{\text{cell},y} l_{\text{cell},z}} \\ k_{e,yy} &= \frac{4A_m k_m}{\sqrt{(l_{\text{cell},x})^2 + (l_{\text{cell},y})^2 + (l_{\text{cell},z})^2}} \frac{l_{\text{cell},y}}{l_{\text{cell},x} l_{\text{cell},z}} \\ k_{e,zz} &= \frac{4A_m k_m}{\sqrt{(l_{\text{cell},x})^2 + (l_{\text{cell},y})^2 + (l_{\text{cell},z})^2}} \frac{l_{\text{cell},z}}{l_{\text{cell},x} l_{\text{cell},y}} \end{aligned} \quad (2)$$

where k_m is the thermal conductivity of the parent material of lattice structure; $l_{\text{cell},x}$, $l_{\text{cell},y}$, and $l_{\text{cell},z}$ are the length of lattice cells in x , y , and z directions, respectively; and $A_m = \pi(r_m)^2$ is the cross-sectional area of lattice members. In this paper, we assume that $l_{\text{cell},x} = l_{\text{cell},y} = l_{\text{cell},z} = l_{\text{cell}}$; however, our discussion can be applied for other cases as well. When $l_{\text{cell},x} = l_{\text{cell},y} = l_{\text{cell},z} = l_{\text{cell}}$, the equivalent thermal conductivity coefficients can be written as

$$k_{e,xx} = k_{e,yy} = k_{e,zz} = k_e = \frac{4A_m}{\sqrt{3}l_{\text{cell}}^2} \cdot k_m \quad (3)$$

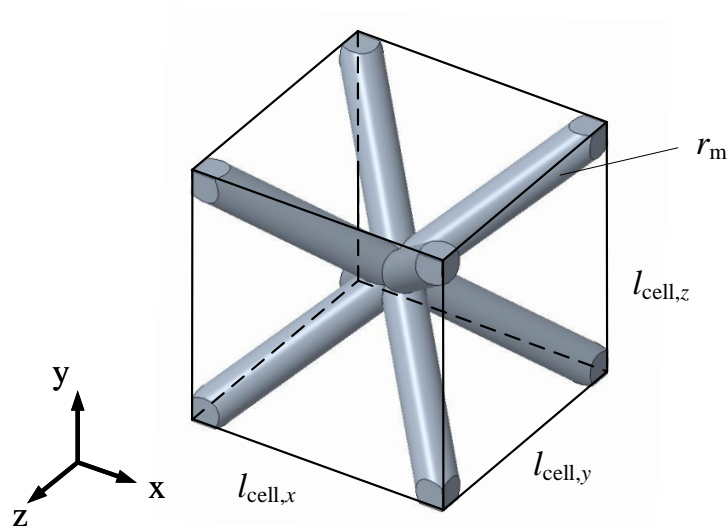


Figure 4. A single cell of BCC type lattice structure.

Then, (1) can be simplified as

$$\frac{\partial^2 T}{\partial x^2} + \frac{\partial^2 T}{\partial y^2} + \frac{\partial^2 T}{\partial z^2} + \frac{\dot{q}}{k_e} = \frac{\rho_e c_e}{k_e} \frac{\partial T}{\partial \tau} \quad (4)$$

where the equivalent density ρ_e can be approximately given as

$$\rho_e \approx \frac{4\sqrt{3}\pi l_{\text{cell}}(r_m)^2 - 39.2(r_m)^3}{(l_{\text{cell}})^3} \rho_m \quad (5)$$

When the temperature variation in each lattice cell is much smaller than that of the whole structure, the heat flux of convective heat transfer in lattice cells can be regarded as constant and occurring at the center of cell; therefore, the process of convective heat transfer is determined by Newton's law of cooling:

$$\Phi_c = h(T_{wf} - T_{lat})A_c \quad (6)$$

where Φ_c is heat transferred by convection per unit time; T_{wf} and T_{lat} are temperature of working fluid and lattice, respectively; h is the convective heat transfer coefficient; and A_c is the area of the interface between the lattice cell and the working fluid.

In the working process described in Section 1, as the heat conduction effect of the working fluid itself is significantly less than that of the structure, the convective heat transfer between the structure and the working fluid can be considered as the only heat input of the working fluid. When $\tau = \tau_0$, the approximate expression of the working fluid temperature at the position of the i -th lattice cell can be written as

$$T_{wf,i}|_{\tau=\tau_0} = T_{wf,i}|_{\tau=\tau_0-\Delta\tau_0} + \frac{h(T_{wf,i}|_{\tau=\tau_0-\Delta\tau_0} - T_{lat,i}|_{\tau=\tau_0-\Delta\tau_0})A_{c,i}}{\rho_{wf}c_{wf}V_{wf,i}}\Delta\tau_0 \quad (7)$$

where ρ_{wf} is the density of working fluid, c_{wf} is the specific heat capacity of working fluid, and $V_{wf,i}$ is the actual volume of working fluid in the i -th lattice cell.

For the BCC type lattice structure, the volume of working fluid, the convective heat transfer contact area, and the equivalent density of working fluid in the i -th lattice cell can be, respectively, given as

$$V_{wf,i} \approx (l_{cell})^3 - 4\sqrt{3}\pi l_{cell}(r_{m,i})^2 + 39.2(r_{m,i})^3 \quad (8)$$

$$A_{c,i} \approx 43.53r_{m,i}l_{cell} - 117.6(r_{m,i})^2, (i = 1, 2, \dots, N) \quad (9)$$

$$\rho_{wfe,i} \approx \left(1 - 21.8\left(\frac{r_{m,i}}{l_{cell}}\right)^2 + 39.2\left(\frac{r_{m,i}}{l_{cell}}\right)^3\right)\rho_{wf}, \quad (i = 1, 2, \dots, N) \quad (10)$$

According to the above model, it can be found that when the structure material and working fluid of lattice structure are given, the working process of the lattice is mainly affected by the type and size of lattice structure. However, in an actual situation, the $l_{cell,x}$, $l_{cell,y}$ and $l_{cell,z}$ of lattice cell is limited by the size of structure and manufacturing process. Therefore, the design of $r_{m,i}$ for each lattice cell is the main topic of this study. In the following, we develop a leaf vein-inspired bionic design method to determine the values of $r_{m,i}$ for all lattice cells to improve the performance of the heat exchanger.

2.2. Leaf Vein Model

In order to realize the bionic design of lattice structure, by observing the growth law of leaf vein, this paper presents a parametric model to describe the growth features of leaf vein. The parametric model describing the growth features of leaf vein is shown in Figure 5, and the parameters are listed as follows:

$$\begin{cases} \mathbf{V} = [\mathbf{v}_0, \mathbf{v}_1, \dots, \mathbf{v}_{n_v-1}]^T \\ \mathbf{c} = [x_c, y_c]^T \\ n_s \\ \mathbf{\Theta} = [\theta_1, \theta_2, \dots, \theta_{n_s-1}]^T \\ \mathbf{\Gamma} = [\gamma_1, \gamma_2, \dots, \gamma_{n_s}]^T \\ \mathbf{D} = [d_1, d_2, \dots, d_{n_s}]^T \end{cases} \quad (11)$$

where \mathbf{V} represents the vertices on the edges of the vein model; $\mathbf{v}_i = [x_{vi}, y_{vi}]^T$, ($i = 1, 2, \dots, n$) is the coordinates of the i -th vertex—two adjacent vertices represent an edge, all the edges form the envelope of the vein model; \mathbf{c} is the root of the vein model and vein “grow” from this position; n_s is the number of stages of veins; θ_j ($j = 1, 2, \dots, n_s - 1$) and γ_k ($k = 1, 2, \dots, n_s - 1$) represent the bifurcation angle and position of each stage of veins; and d_l ($l = 1, 2, \dots, n_s$) is the diameter of each stage of veins.

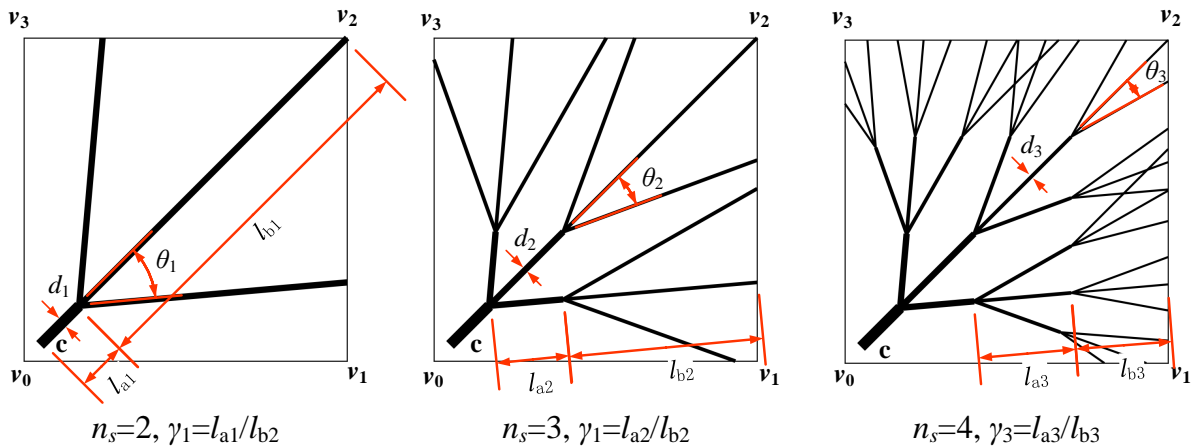


Figure 5. Parametric model describing the growth features of leaf vein.

When the above main parameters vary, the model also changes accordingly, for instance, when n_s , Θ and Γ take different values, the generated models are shown in Figure 6.

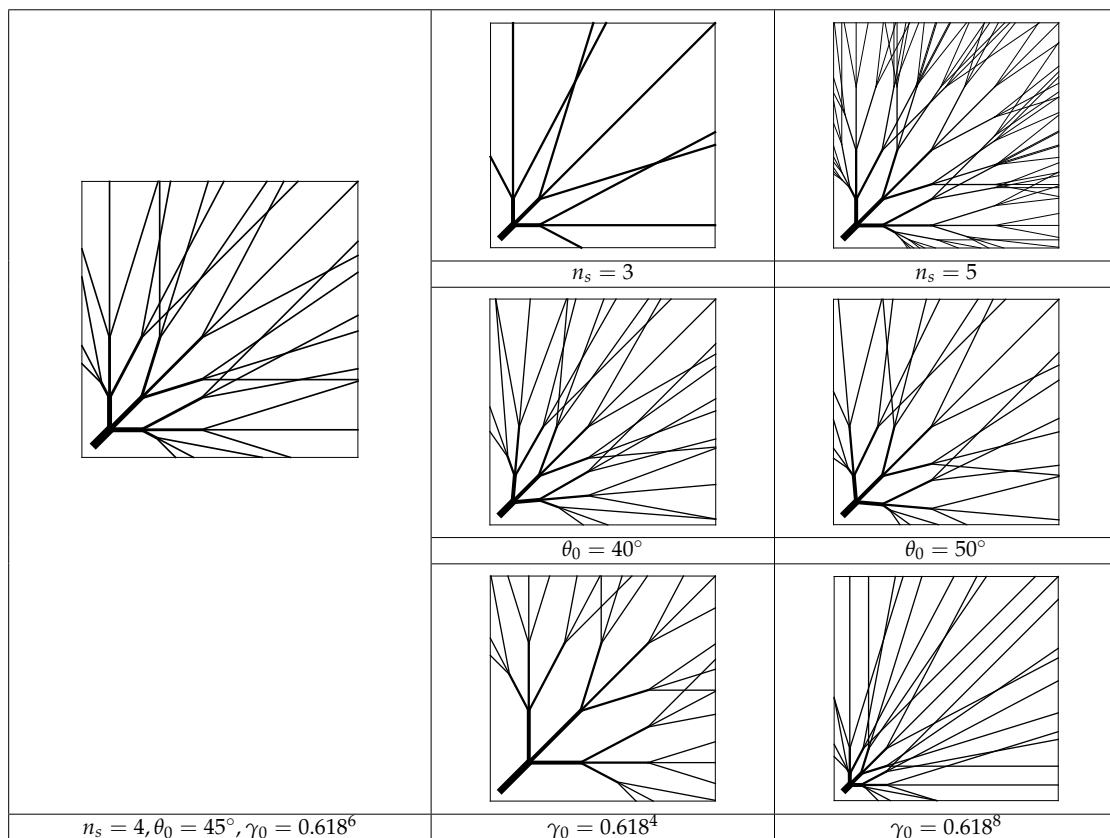


Figure 6. Proposed leaf veins model. NOTE: In the above model, Θ and Γ satisfy the relation of $\theta_i = 0.618 \times \theta_{i-1}$ and $\gamma_i = 0.618^2 \times \gamma_{i-1}$ [29].

2.3. Mapping Method

After the leaf vein model is generated according to size of exchanger and working conditions, the leaf vein model is mapped to the lattice structure by the following method to generate the bionic design of the lattice structure. First, the 3D grids of the lattice structure are reduced to 2D grids on the x-y plane (Figure 7a); then, the collections of 2D grids that each stage of leaf veins pass through are obtained (Figure 7b) and named 'k-th collection' ($k = 1, 2, \dots, n_s$), and grids that are not mapped by any leaf veins are set as a collection named '($n_s + 1$)-th collection'. Finally, the collections of 3D lattice structure are obtained according to the collections of 2D grids (Figure 7c), thus the lattice structure cells are divided into different collections according to the distribution characteristics of leaf veins. The lattice structure cells in a collection have the same radii.

Assume that the relationship between the radii of the lattice structure from collection of different stages is geometric series and the material of the lattice structure is prescribed, then the above mass constraints can be written as

$$\sum_k^{n_s+1} \left(n_k \left(4\sqrt{3}\pi l_{\text{cell}} \left(r_0 \beta^{n_s-k+1} \right)^2 - 39.2 \left(r_0 \beta^{n_s-k+1} \right)^3 \right) \right) = V_{\text{uni}} \quad (12)$$

where r_0 is the minimum radius value of whole lattice structure as well as the lattice cells which are not mapped by any leaf veins, β is the ratio of the radii of adjacent stages collections, V_{uni} is the prescribed volume of the materials constituting the lattice structure, and n_k is the count of lattice cells in k-th collection.

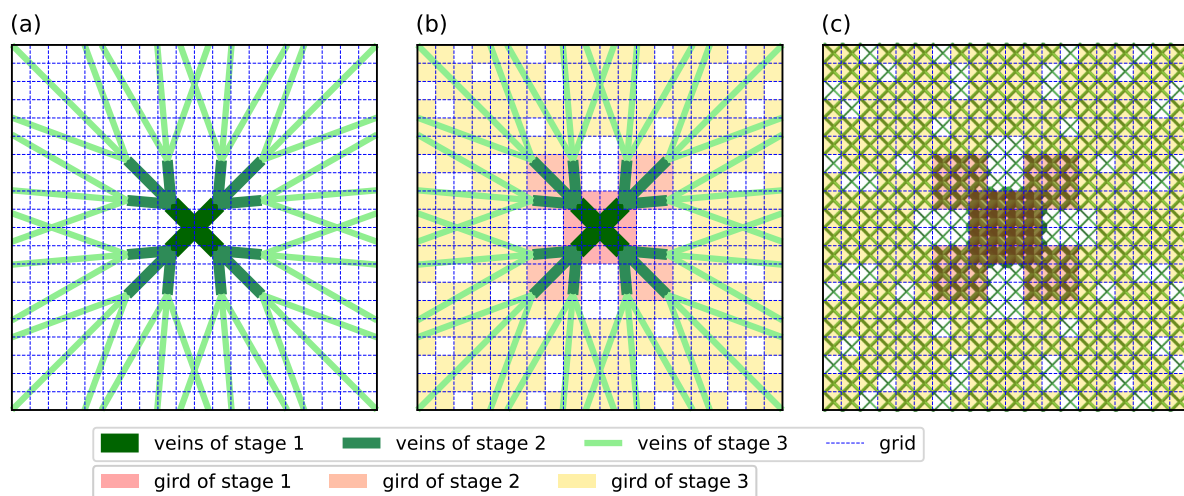


Figure 7. Bionic model mapping design method. (a) 2D grids of lattice structure. (b) 2D grids collections of different stages. (c) 3D lattice structure collections obtained by 2D grids collections.

3. Uniform and Bionic Designs

3.1. Working Conditions and Uniform Design

The working conditions and design constraints are as follows: the size of the inner cavity of the heat exchanger is $L_x \times L_y \times L_z = 200 \times 200 \times 20 \text{ mm}^3$. The materials of the structure and working fluid are aluminum and liquid, respectively. The initial temperature of the whole exchanger is $T_0 = 273.15 \text{ K}$. Convective heat transfer coefficient is $h = 10,000 \text{ W}/(\text{m}^2 \cdot \text{K})$. Two working conditions are considered in this work:

WC₁: The temperature at the center of the lattice structure is a constant value of $T_0 = 323.15 \text{ K}$.

WC₂: A constant heat sink of $T_{\text{sink}} = 323.15 \text{ K}$ is applied at the center of the lattice structure and the heat is continuously transferred to the structure. The heat conduction area and coefficient are $A_{\text{sink}} = 100 \text{ mm}^2$ and $h_{\text{sink}} = 20,000 \text{ W}/(\text{m}^2 \cdot \text{K})$, respectively.

Considering the influence of design parameters of lattice structure on the performance of the exchanger, two uniform designs of lattice structure U_1 and U_2 with parameters listed in Table 1 are employed to demonstrate the performance advantage of the bionic designs.

Table 1. The parameters of uniform design models.

| Parameters | Uniform Design 1 (U_1) | Uniform Design 2 (U_2) |
|---|----------------------------|----------------------------------|
| $\mathbf{R} = [r_{m,1}, r_{m,2}, \dots, r_{m,N}]^T / \text{mm}$ | $[1.0, 1.0, \dots, 1.0]^T$ | $[0.667, 0.667, \dots, 0.667]^T$ |
| $l_{\text{cell}} / \text{mm}$ | 10.0 | 6.667 |
| M / kg | 0.397 | 0.397 |
| N | 800 | 2700 |

3.2. Bionic Design Inspired by Leaf Veins

According to the working conditions and design conditions described in Section 3.1, the leaf veins model shown in Figure 8 can be established, where the values of \mathbf{V} are determined by the dimensions of the heat exchanger in the x and y directions, the value of c is determined by the location of the central thermal loads, $n_s = 3$, and Θ and Γ are given as

$$\begin{cases} \theta_0 = 40^\circ \\ \theta_i = \theta_{i-1} \times 0.618 \\ \gamma_0 = (0.618)^4 \\ \gamma_i = \gamma_{i-1} \times 0.618 \end{cases} \quad (i = 1, 2) \quad (13)$$

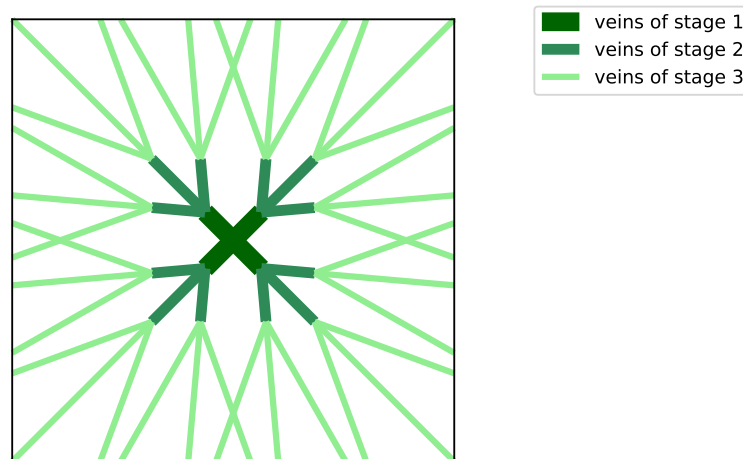


Figure 8. Leaf vein model for two working conditions.

Then, graded lattice structures, instead of uniform lattice structures, can be generated based on the leaf vein model described in Equation (13) and the mapping method developed in Section 2.3.

Accordingly, two bionic designs, B_1 and B_2 , corresponding to the uniform designs can be obtained. The values of the parameters of r_0 and other parameters are shown in Table 2. where the value of beta and the radii of lattice in difference collections of stages are obtained according to Equation (12).

Table 2. The parameters of bionic design models.

| Parameters | Bionic Design 1 (B_1) | Bionic Design 2 (B_1) |
|--|---------------------------------|----------------------------------|
| $[N_{s1}, N_{s2}, N_{s3}, N_{s4}]^T$ | $[32, 64, 560, 144]^T$ | $[48, 192, 1380, 1080]^T$ |
| r_0 / mm | 0.5 | 0.4 |
| β | 1.793 | 1.746 |
| $[r_{s1}, r_{s2}, r_{s3}, r_{s4}]^T / \text{mm}$ | $[2.882, 1.607, 0.8965, 0.5]^T$ | $[2.1305, 1.220, 0.6986, 0.4]^T$ |

Due to the different densities of the lattice, when the same leaf vein model is mapped to the lattice structure, different lattice structure collections are obtained as shown in Figure 9. Compared with B_1 , the number of 2D grids in B_2 is increased from 400 to 900, as well as the number of lattice cells being increased from 800 to 2700, the mapping process is more refined and the mapping results are more obvious when showing the distribution characteristics of the leaf vein model. Through the comparison of the lattice cells number in collections, the proportion of the grids in the 4th collection, that is, the grids that are not penetrated by any leaf veins, has increased significantly, leading to the change of the mass proportion of lattice structure in each collection.

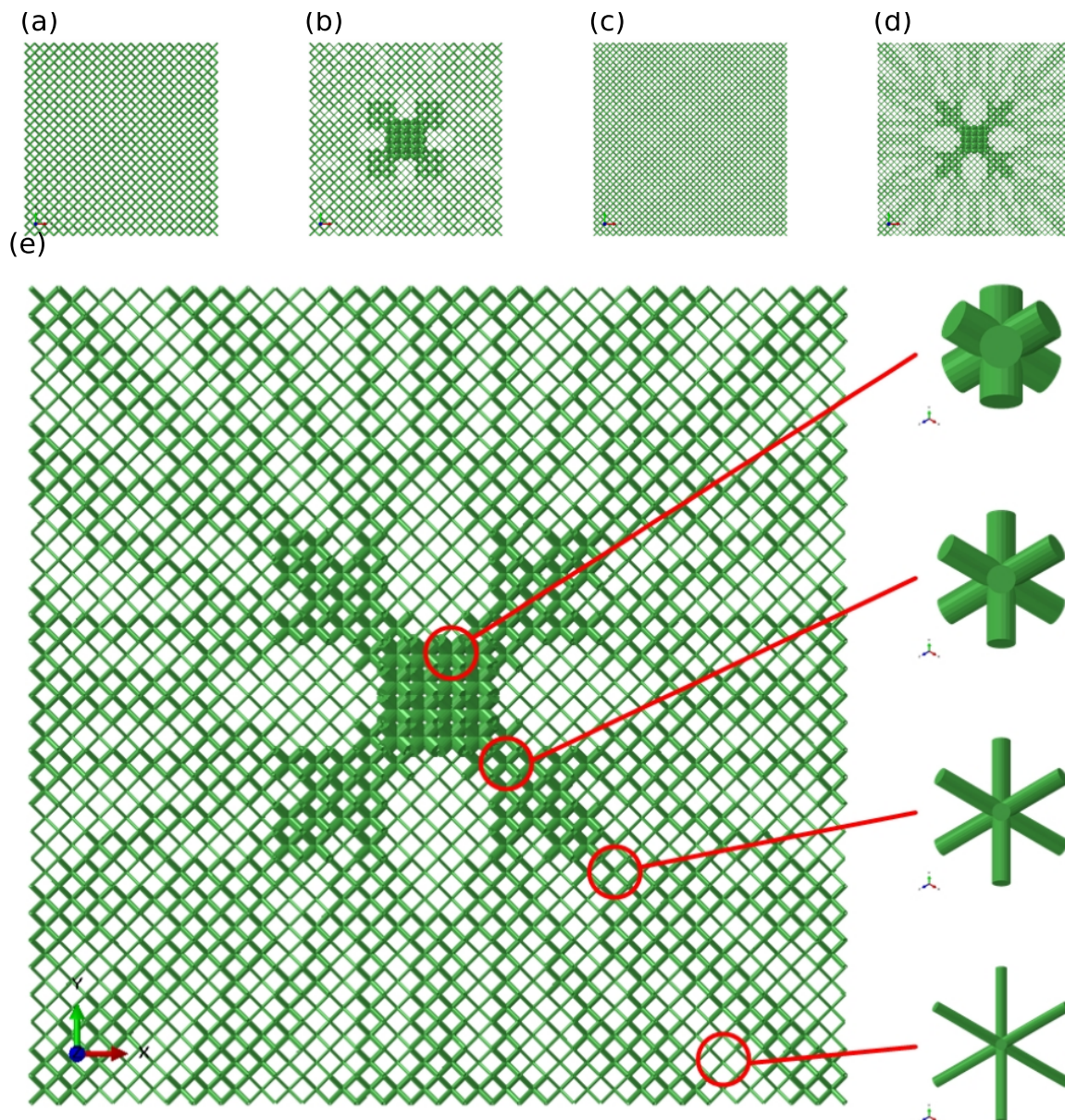


Figure 9. Uniform designs and Bionic designs obtained by mapping methods. (a,b) U_1 and B_1 with $l_{\text{cell}} = 10.0\text{mm}$. (c,d) U_2 and B_2 with $l_{\text{cell}} = 6.667\text{mm}$. (e) Lattices with different size in B_2 .

4. Results and Discussion

In order to verify the effectiveness of the bionic design method, finite element analysis is carried out to demonstrate the performance advantage of the bionic design over the uniform lattice design.

4.1. Finite Element Model

Based on the mathematical model described in Section 2.1, a finite element model of heat exchanger is established. As shown in Figure 10, each member of lattice structure is modeled as a one-dimensional element and working fluid is modeled by continuous three-dimensional solid elements. In addition, although the lattice structure and the working fluid model are separately established in space, the convective heat transfer between the lattice cells and the corresponding working fluid are considered by Equation (6)

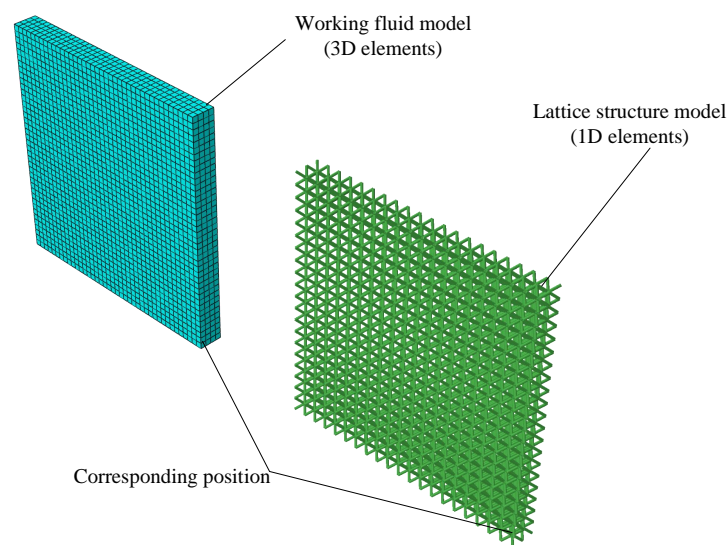


Figure 10. Finite element model.

Due to the use of two-dimensional element to simulate the members of each lattice cell, the mass of each lattice element needs to be corrected. The mass correction coefficient of each lattice cell is given as

$$c_c = \frac{4\sqrt{3}\pi l_{\text{cell}} - 39.2r_{m,i}}{4\sqrt{3}\pi l_{\text{cell}}} \quad (14)$$

For structures with constant mass and working fluid mass and working conditions above, the steady-state state is the same. Therefore, we take the first 1200 s before the structure reaches a steady state to observe the heat transferred from the structure to the working fluid.

4.2. Working Condition 1

The analysis results transient heat transfer process of U_1 and B_1 under WC_1 are shown in Figure 11. As the heat transfer process result of U_2 and B_2 are similar to those of U_1 and B_1 , the results of U_2 and B_2 are not shown here. Intuitively, during the heat transfer process of the first 1200 s, the heat is gradually transferred from the center of the lattice structure to the edges in both designs, the temperature of the working fluid gradually increases due to the convective heat transfer process, and its temperature distribution is similar to the lattice structure. However, at the end of 1200 s, the temperature of edge position of the lattice structure in U_1 is still at a value close to the initial temperature.

Two indicators are used to evaluate the heat transfer capacity of the heat exchanger: the average temperature increment of lattice structure ΔT_{ave} and the total value of heat transferred from the structure to the working fluid Q_c in the simulation process. The higher values of the two indicators, the better the heat transfer and heat dissipation performance of the structure.

The numerical values of ΔT_{ave} and Q_c are plotted in Figure 12a,b. It can be observed that the bionic design has a significant increase in both indicators when compared with the uniform design during the working process, indicating that the heat has a higher transfer efficiency in the lattice structure of the bionic design.

4.3. Working Condition 2

The heat transfer process results of U_1 and B_1 under WC_2 are shown in Figure 13, and the values of ΔT_{ave} and Q_c are shown in Figure 12c,d and Table 3.

It can be found that under WC_2 , the center of the uniform design is continuously heated to a temperature closer to $T_{sink} = 323.15$ K, but the heat is not effectively diffused to other positions of the lattice structure. On the other hand, due to the gradient of the lattice structure of bionic design, the heat in the center of the lattice structure is effectively transferred to other positions, which means that the temperature of the lattice structure central T_{center} of bionic design is continuously lower than the uniform design and ensures the effective absorption of heat from heat sink to achieve the purpose of heat dissipation. Thus, the heat transfer efficiency of the bionic design is obviously higher than that of the uniform lattice design.

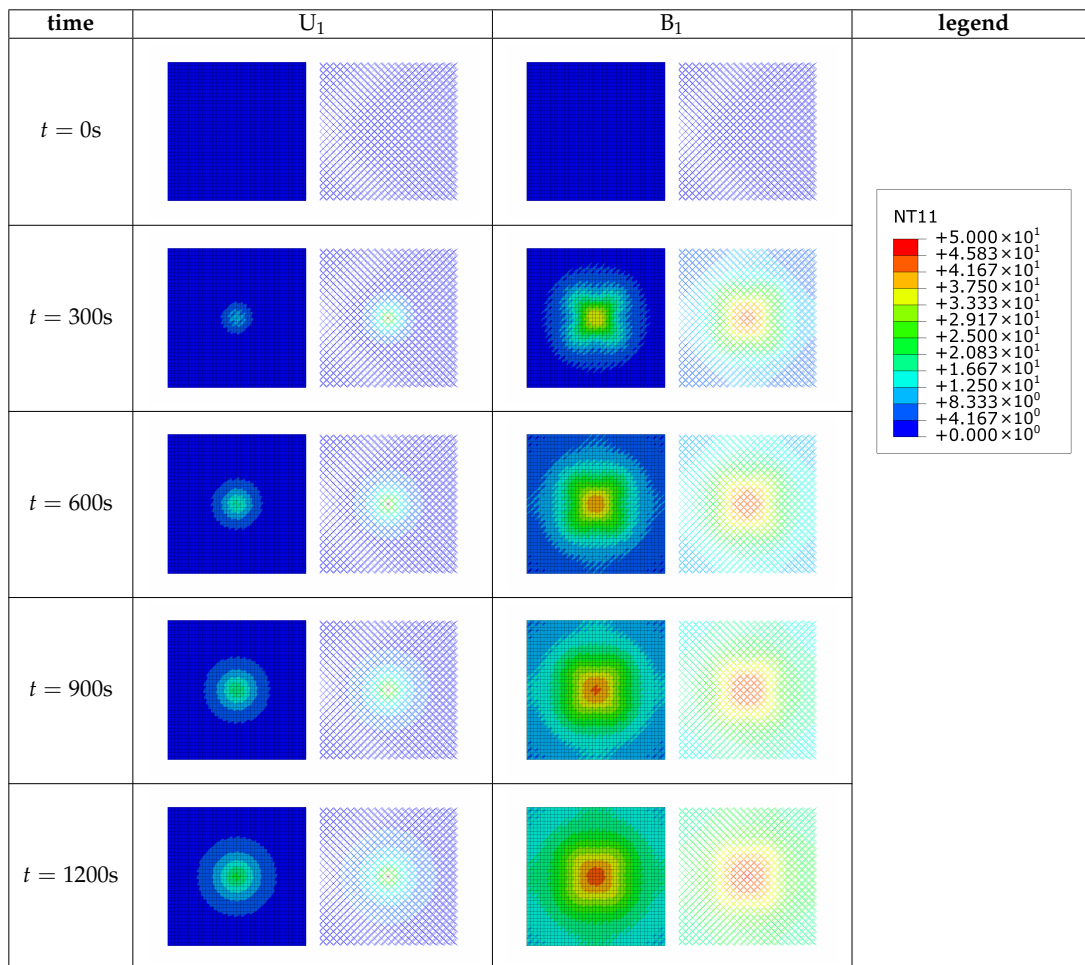


Figure 11. Transient heat transfer process analysis results of U_1 and B_1 under WC_1 .

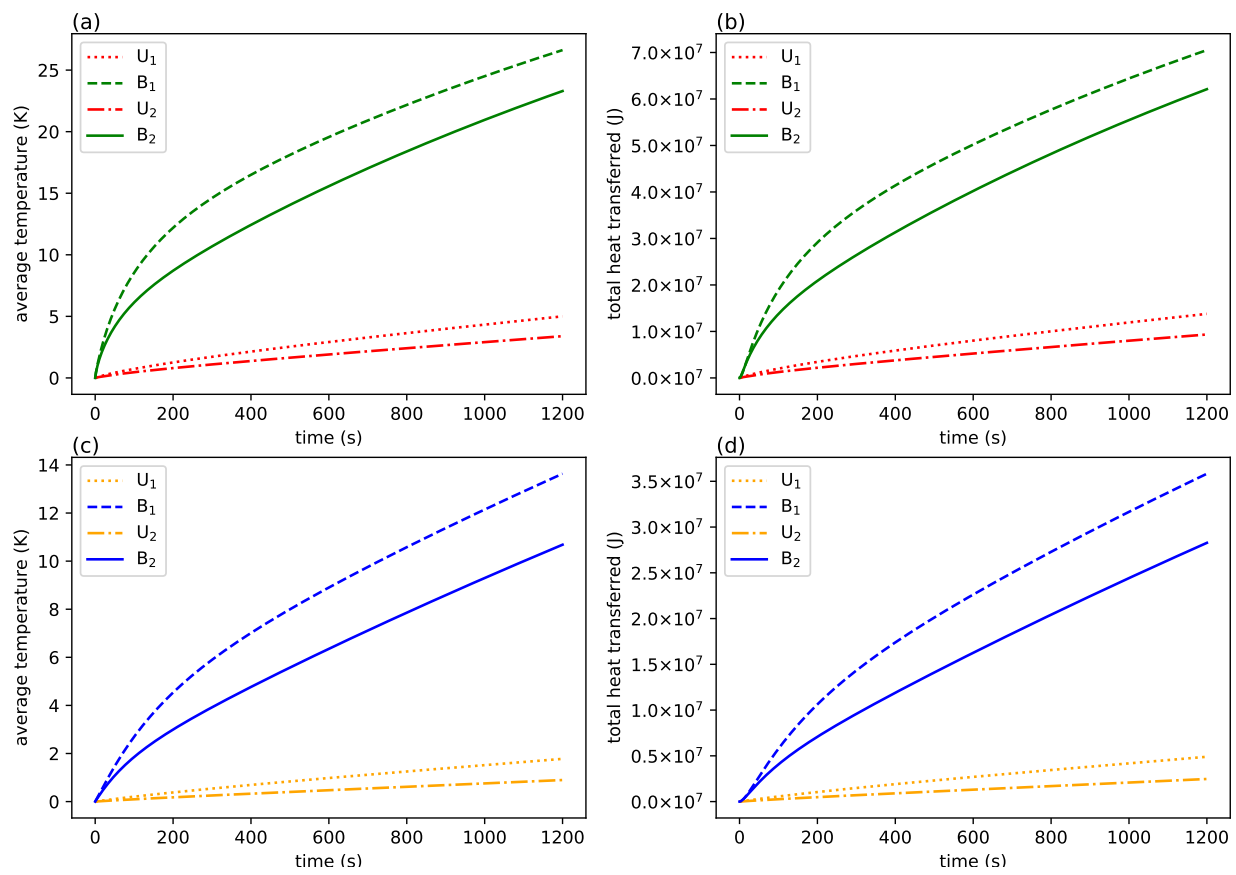


Figure 12. Comparison of numerical simulation results of uniform design and bionic design. (a,b) ΔT_{ave} and Q_c of WC₁; (c,d) ΔT_{ave} and Q_c of WC₂.

Table 3. The value of ΔT_{ave} and Q_c of both designs under 2 working conditions.

| Designs | WC ₁ | | WC ₂ | |
|----------------|--------------------|---------|--------------------|---------|
| | $\Delta T_{ave}/K$ | Q_c/J | $\Delta T_{ave}/K$ | Q_c/J |
| U ₁ | 5.001 | 13,780 | 1.777 | 4897 |
| B ₁ | 26.625 | 70,517 | 13.634 | 35,825 |
| ratio | 5.32 | 5.12 | 7.67 | 7.31 |
| U ₂ | 3.390 | 9344 | 0.896 | 2469 |
| B ₂ | 23.298 | 62,106 | 10.683 | 28,275 |
| ratio | 6.87 | 6.65 | 11.91 | 11.44 |

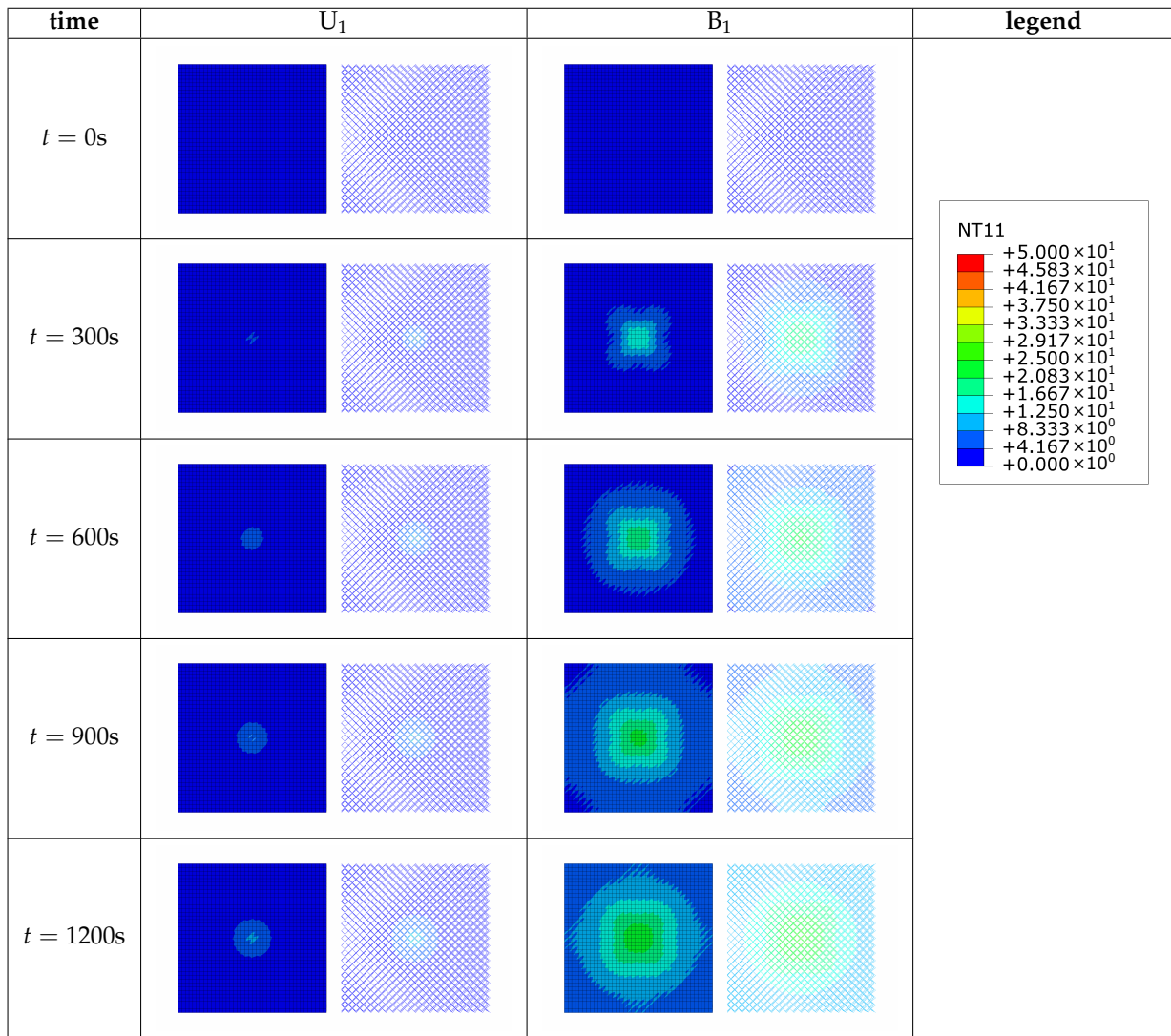


Figure 13. Transient heat transfer process analysis results of U_1 and B_1 under WC_2 .

4.4. Comparison of Heat Transfer Efficiency

In order to clearly compare the heat transfer efficiency between the uniform and the bionic designs, the required time τ_r for the bionic structure to transfer the total heat transferred by the uniform structure within 1200 s is calculated. The results are shown in Figure 14. Note that compared with the uniform design, the bionic design greatly shortens the time required to transfer the same heat. In the four cases listed in this work, the bionic design B_1 under WC_2 takes the longest time to transfer the corresponding heat, which is 85 s and corresponds to only 7.08% of 1200 s, demonstrating that bionic design can improve the heat transfer efficiency of the heat exchanger.

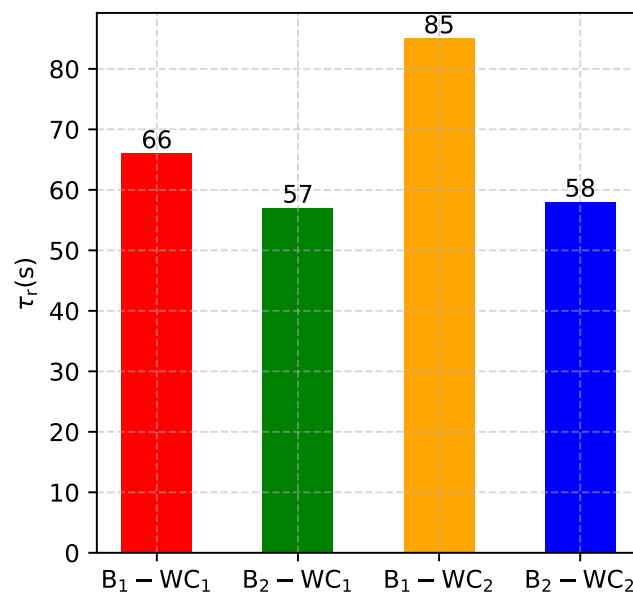


Figure 14. The value of τ_r of bionic designs under 2 working conditions.

4.5. Comparison between B₁ and B₂

In both working conditions, by changing the mass distribution of lattice structure the bionic design has brought a significant improvement in the heat transfer performance of the structure. Although the steady state of all designs are the same, the values of ΔT_{ave} and Q_c in the first 1200 s are different. The ratios of the two bionic structures relative to the uniform design are also shown in Table 3. Although the indicators of B₂ are lower than that of B₁, relative to uniform design, B₂ has a higher percentage improvement and lower τ_r value. This demonstrates that the refined bionic design is more effective in heat transfer; a further indication of the effectiveness of the method proposed in this work.

5. Conclusions

To further improve the heat dissipation efficiency of the lattice structure infill heat exchanger, this paper developed a leaf vein-inspired bionic design method for heat exchanger infilled with graded lattice structure. In order to realize the bionic design, we propose a model to describe the vein model and a mapping method to generate graded lattice structures according to the leaf vein models. Several transient thermal analyses are conducted under two types of central thermal loads to analyze and compare the heat transfer and heat dissipation performance of uniform designs and bionic designs. Conclusions are summarized as follows.

(1) According to the changes in the temperature cloud diagram of the analysis results, it can be seen that the heat transfer process of the bionic design and the uniform design both are spread from the center to the edge, but the bionic design has a higher diffusion rate, especially in the second working condition where the advantages of bionic design are more obvious.

(2) The numerical values of ΔT_{ave} , Q_c , and τ_r in the analysis result indicate that the performance of the bionic design is significantly better than the uniform design under the two working conditions. Under the condition of constant mass, it takes less time for the bionic design to transfer the same heat than uniform design, thereby significantly improving the heat transfer efficiency of the heat exchanger.

(3) The same leaf vein model combined with different lattice structures can obtain different bionic design results. When the number of lattice structure cells is increased, a more refined bionic design can be produced. Comparing different bionic designs, the performance improvement ratio of fine bionic design is higher, which further demonstrates the role of bionic design in improving the performance of the structure.

(4) In many fields, especially aerospace, heat exchangers infilled with uniform lattice structure have practical applications [30–32]. The mass distribution of the lattice structure can be changed reasonably based on the proposed method, and the simulation results show that the heat dissipation performance of the structure is effectively improved. Thus, the leaf vein-inspired bionic design method has great application prospects.

Author Contributions: Conceptualization, H.D. and J.Z.; methodology, H.D.; software, H.D.; validation, H.D., J.Z. and C.W.; formal analysis, H.D.; investigation, H.D. and J.Z.; resources, C.W.; data curation, H.D.; writing—original draft preparation, H.D.; writing—review and editing, H.D. and J.Z.; visualization, H.D.; supervision, C.W.; project administration, C.W.; funding acquisition, C.W. All authors have read and agreed to the published version of the manuscript.

Funding: This research was supported by the National Natural Science Foundation of China (Grant No51635002).

Conflicts of Interest: The authors declare no conflict of interest.

References

1. Ashby, M.; Cebon, D. Materials Selection in Mechanical Design. *J. Phys. IV Proc.* **1993**, *3*, C7-1–C7-9. [[CrossRef](#)]
2. Feng, S.S.; Li, M.Z.; Joo, J.H.; Kang, K.J.; Kim, T.; Lu, T.J. Thermomechanical Properties of Brazed Wire-Woven Bulk Kagome Cellular Metals for Multifunctional Applications. *J. Thermophys. Heat Transf.* **2012**, *26*, 66–74. [[CrossRef](#)]
3. Yan, H.B.; Zhang, Q.C.; Lu, T.J.; Kim, T. A Lightweight X-Type Metallic Lattice in Single-Phase Forced Convection. *Int. J. Heat Mass Transf.* **2015**, *83*, 273–283. [[CrossRef](#)]
4. Joo, J.H.; Kang, K.J.; Kim, T.; Lu, T.J. Forced Convective Heat Transfer in All Metallic Wire-Woven Bulk Kagome Sandwich Panels. *Int. J. Heat Mass Transf.* **2011**, *54*, 5658–5662. [[CrossRef](#)]
5. Kim, T.; Zhao, C.Y.; Lu, T.J.; Hodson, H.P. Convective Heat Dissipation with Lattice-Frame Materials. *Mech. Mater.* **2004**, *36*, 767–780. [[CrossRef](#)]
6. Maloney, K.J.; Fink, K.D.; Schaedler, T.A.; Kolodziejska, J.A.; Jacobsen, A.J.; Roper, C.S. Multifunctional Heat Exchangers Derived from Three-Dimensional Micro-Lattice Structures. *Int. J. Heat Mass Transf.* **2012**, *55*, 2486–2493. [[CrossRef](#)]
7. Ranut, P. On the Effective Thermal Conductivity of Aluminum Metal Foams: Review and Improvement of the Available Empirical and Analytical Models. *Appl. Therm. Eng.* **2016**, *101*, 496–524. [[CrossRef](#)]
8. Dai, Z.; Nawaz, K.; Park, Y.G.; Bock, J.; Jacobi, A.M. Correcting and Extending the Boomsma–Poulikakos Effective Thermal Conductivity Model for Three-Dimensional, Fluid-Saturated Metal Foams. *Int. Commun. Heat Mass Transf.* **2010**, *37*, 575–580. [[CrossRef](#)]
9. Boomsma, K.; Poulikakos, D. On the Effective Thermal Conductivity of a Three-Dimensionally Structured Fluid-Saturated Metal Foam. *Int. J. Heat Mass Transf.* **2001**, *44*, 827–836. [[CrossRef](#)]
10. Haack, D.; Butcher, K.; Kim, T.; Lu, T. Novel Lightweight Metal Foam Heat Exchangers. *Am. Soc. Mech. Eng. Process. Ind. Div. (Publ.) PID* **2001**, *6*, 1–7.
11. Wang, N.; Kaur, I.; Singh, P.; Li, L. Prediction of Effective Thermal Conductivity of Porous Lattice Structures and Validation with Additively Manufactured Metal Foams. *Appl. Therm. Eng.* **2021**, *187*, 116558. [[CrossRef](#)]
12. Ho, J.; Leong, K. Cylindrical Porous Inserts for Enhancing the Thermal and Hydraulic Performance of Water-Cooled Cold Plates. *Appl. Therm. Eng.* **2017**, *121*, 863–878. [[CrossRef](#)]
13. Ho, J.Y.; Leong, K.C.; Wong, T.N. Experimental and Numerical Investigation of Forced Convection Heat Transfer in Porous Lattice Structures Produced by Selective Laser Melting. *Int. J. Therm. Sci.* **2019**, *137*, 276–287. [[CrossRef](#)]
14. Shen, B.; Li, Y.; Yan, H.; Boetcher, S.K.S.; Xie, G. Heat Transfer Enhancement of Wedge-Shaped Channels by Replacing Pin Fins with Kagome Lattice Structures. *Int. J. Heat Mass Transf.* **2019**, *141*, 88–101. [[CrossRef](#)]
15. Deng, H.; Wang, C. Equivalent thermal analysis and optimization method for three-dimensional lattice structure. *J. Beijing Univ. Aeronaut. Astronaut.* **2019**, *45*, 1122–1128.
16. Sypeck, D.J. Cellular Truss Core Sandwich Structures. *Appl. Compos. Mater.* **2005**, *12*, 229–246. [[CrossRef](#)]
17. Yan, H.B.; Zhang, Q.C.; Lu, T.J. An X-Type Lattice Cored Ventilated Brake Disc with Enhanced Cooling Performance. *Int. J. Heat Mass Transf.* **2015**, *80*, 458–468. [[CrossRef](#)]
18. Qi, C.; Wang, Y.; Tang, J. Effect of Squid Fin Bionic Surface and Magnetic Nanofluids on CPU Cooling Performance under Magnetic Field. *Asia-Pac. J. Chem. Eng.* **2020**, *15*, e2482. [[CrossRef](#)]
19. Liang, Y.; Liu, P.; Zheng, N.; Shan, F.; Liu, Z.; Liu, W. Numerical Investigation of Heat Transfer and Flow Characteristics of Laminar Flow in a Tube with Center-Tapered Wavy-Tape Insert. *Appl. Therm. Eng.* **2019**, *148*, 557–567. [[CrossRef](#)]
20. Dey, P.; Hedau, G.; Saha, S.K. Experimental and Numerical Investigations of Fluid Flow and Heat Transfer in a Bioinspired Surface Enriched Microchannel. *Int. J. Therm. Sci.* **2019**, *135*, 44–60. [[CrossRef](#)]
21. Huang, P.; Dong, G.; Zhong, X.; Pan, M. Numerical Investigation of the Fluid Flow and Heat Transfer Characteristics of Tree-Shaped Microchannel Heat Sink with Variable Cross-Section. *Chem. Eng. Process.—Process. Intensif.* **2020**, *147*, 107769. [[CrossRef](#)]

22. Xu, S.; Li, Y.; Hu, X.; Yang, L. Characteristics of Heat Transfer and Fluid Flow in a Fractal Multilayer Silicon Microchannel. *Int. Commun. Heat Mass Transf.* **2016**, *71*, 86–95. [[CrossRef](#)]
23. Xu, S.; Wang, W.; Fang, K.; Wong, C.N. Heat Transfer Performance of a Fractal Silicon Microchannel Heat Sink Subjected to Pulsation Flow. *Int. J. Heat Mass Transf.* **2015**, *81*, 33–40. [[CrossRef](#)]
24. Zhang, D.y.; Luo, Y.h.; Li, X.; Chen, H.w. Numerical Simulation and Experimental Study of Drag-Reducing Surface of a Real Shark Skin. *J. Hydrodyn. Ser. B* **2011**, *23*, 204–211. [[CrossRef](#)]
25. Žemaitis, A.; Mikšys, J.; Gaidys, M.; Gečys, P.; Gedvilas, M. High-Efficiency Laser Fabrication of Drag Reducing Riblet Surfaces on Pre-Heated Teflon. *Mater. Res. Express* **2019**, *6*, 065309. [[CrossRef](#)]
26. Bai, Q.; Bai, J.; Meng, X.; Ji, C.; Liang, Y. Drag Reduction Characteristics and Flow Field Analysis of Textured Surface. *Friction* **2016**, *4*, 165–175. [[CrossRef](#)]
27. Zhao, Y.; Wang, C.; Huang, H.; Ma, R. Heat transfer performance of flat-plate heat pipe with bionic vein microstructure surface. *J. Therm. Sci. Technol.* **2019**, *18*, 471–475.
28. Zhang, Q.; Han, Y.; Chen, C.; Lu, T. Ultralight X-Type Lattice Sandwich Structure (I): Concept, Fabrication and Experimental Characterization. *Sci. China Ser. E Technol. Sci.* **2009**, *52*, 2147–2154. [[CrossRef](#)]
29. Sun, Z.; Cui, T.; Zhu, Y.; Zhang, W.; Shi, S.; Tang, S.; Du, Z.; Liu, C.; Cui, R.; Chen, H.; et al. The Mechanical Principles behind the Golden Ratio Distribution of Veins in Plant Leaves. *Sci. Rep.* **2018**, *8*, 13859. [[CrossRef](#)] [[PubMed](#)]
30. Zhou, H.; Zhang, X.; Zeng, H.; Yang, H.; Lei, H.; Li, X.; Wang, Y. Lightweight Structure of a Phase-Change Thermal Controller Based on Lattice Cells Manufactured by SLM. *Chin. J. Aeronaut.* **2019**, *32*, 1727–1732. [[CrossRef](#)]
31. Guo, Y.; Yang, H.; Fu, W.; Bai, L.; Miao, J. Temperature Control of Star Sensor Baffle Using 3D Printing and PCM Thermal Energy Storage Technology. *Int. J. Heat Mass Transf.* **2021**, *165*, 120644. [[CrossRef](#)]
32. Guo, Y.; Yang, H.; Lin, G.; Jin, H.; Shen, X.; He, J.; Miao, J. Thermal Performance of a 3D Printed Lattice-Structure Heat Sink Packaging Phase Change Material. *Chin. J. Aeronaut.* **2021**, *34*, 373–385. [[CrossRef](#)]